The paper was presented at the Ninth Meeting
"New Trends in Fatigue and Fracture" (NT2F9)
Belgrade, Serbia, 12-14 October 2009

Julian Capelle[1], Joseph Gilgert[1], Ihor Dmytrakh[2], Guy Pluvinage[1]

DEFECT ASSESSMENT ON PIPE USED FOR TRANSPORT OF MIXTURE OF HYDROGEN AND NATURAL GAS

OCENA GREŠKE NA CEVI ZA TRANSPORT MEŠAVINE VODONIKA I PRIRODNOG GASA

Original scientific paper
UDC: 620.193.4:621.643-034.14
620.193.4:669.14-462
Paper received: 10.9.2009

Author's address:
[1)] LaBPS, Ecole Nationale d'Ingénieurs de Metz (ENIM), Ile du Saulcy, Metz, France, capelle@enim.fr
[2)] Karpenko Physico-Mechanical Institute of National Academy of Sciences of Ukraine, Lviv, Ukraine

Keywords
- defect assessment
- pipeline
- gas transport
- mixture of nitrogen and natural gas
- probability of failure

Ključne reči
- ocena greške
- cevovod
- transport gasa
- mešavina vodonika i prirodnog gasa
- verovatnoća otkaza

Abstract

The present article indicates the change of mechanical properties of X52 gas pipe steel in presence of hydrogen and its consequence on defect assessment, particularly on notch-like defects. The purpose is to determine if the transport of a mixture of natural gas and hydrogen in the existing European natural gas pipe network can be done with an acceptable low failure risk (i.e. failure probability less than 10^{-6}). To evaluate the risk, a deterministic defect assessment method has been established, based on Failure Assessment Diagram (FAD), and more precisely on here proposed Modified Notch Failure Assessment Diagram (MNFAD). The MNFAD is coupled with the SINTAP failure curve and enables determining the safety factor associated with defect geometry, loading conditions and material resistance. The paper is performed in the scope of project NATURALHY, part 3 "Durability of pipeline material".

Izvod

Ovaj rad prikazuje promene mehaničkih svojstava čelika za gasovode X52 u atmosferi vodonika i njihov uticaj na ocenu grešaka, posebno na greške tipa zareza. Svrha rada je da se utvrdi da li se za transport mešavine vodonika i prirodnog gasa može sa prihvatljivo niskim rizikom otkaza koristiti postojeća evropska mreža gasovoda (tj. verovatnoća otkaza manja od 10^{-6}). Za ovu procenu je primenjen deterministički pristup, na bazi Dijagrama ocene otkaza (FAD), i preciznije, na u ovom radu predloženom Modifikovanom dijagramu otkaza zbog zareza (MNFAD. Predloženi MNFAD je objedinjen sa SINTAP krivom otkaza i omogućava određivanje faktora sigurnosti prema geometrijskom obliku greške, uslovima opterećenja i otpornosti materijala. Prikazani rad je ostvaren kao sastavni deo projekta NATURALHY u okviru odeljka 3 „Vek materijala za cevovode".

INTRODUCTION

European Gas Network

The European gas pipelines network plays an important role for national economies and at a global level in Europe. This importance will permanently increase with prospective plans of introducing European hydrogen energy infrastructure, /1, 2/, and possible use of existing pipeline networks for transportation of natural gas and hydrogen mixtures. Within the European project NATURALHY /3/, 39 European partners have combined their efforts to assess the effects of the presence of hydrogen on the existing gas network. Key issues are durability of pipeline material, integrity management, safety aspects, life cycle and socio-economic assessment. The work described in this paper was performed within the NATURALHY work package "Durability of pipeline material". The causes of failures in gas pipelines are of various nature, Fig. 1.

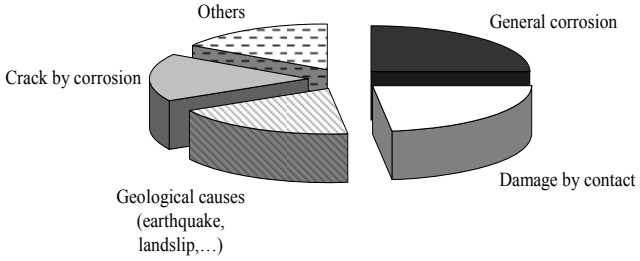

Figure 1. Causes of fracture of pipelines in exploitation, /4/.
Slika 1. Uzroci loma cevovoda u eksploataciji

They can appear by fracture or by leak, what also depends of the nature of the transported fluid. The majority

of these failures are caused by pitting corrosion or cracking by stress corrosion, but there are also problems related to weld defects. Ground movement (landslide, earthquake) can also be the cause of damage on buried pipelines. The owners of pipelines study these problems for a long time and have a good knowledge of methods allowing for their management.

External mechanical loads are the cause of many problems, Fig. 1. Indeed, it happens that pipelines are damaged or perforated accidentally at time of excavation work. Crack initiation in, and rupture, emanating from stress concentration are at the origin of more than 90% of service failures. Presence of geometric discontinuity such as a notch will reduce the fracture resistance of the pipeline and the cross section of pipe wall, making it more sensitive to operating pressure and loads caused by ground movement. In this paper, authors developed a new approach based on Failure Assessment Diagram (FAD), Structural INTegrity Assessment Procedure for the European industry (SINTAP), and the Volumetric Method. This tool allows to assess the harmfulness of a notch type defect, by using two factors: the security factor and the safety factor.

Steel used

The studied steel, API 5L X52, is the most common gas pipeline material for transport of oil and gas during 1950-1960. The standard chemical composition and mechanical properties of this steel are shown in Tables 1 and 2.

Table 1. Chemical composition of X52 steel (mass, %).
Tabela 1. Hemijski sastav čelika X52 (mas. %)

C	Mn	Si	Cr	Ni	Mo	S	Cu	Ti	Nb	Al
0.116	1.29	0.27	0.06	0.033	0.01	0.001	0.024	0.003	<0.02	0.034

Table 2. Mechanical properties of X52 steel, /5/.
Tabela 2. Mehaničke osobine čelika X52, /5/

E, GPa	σ_Y, MPa	σ_U , MPa	A, %	n	K, MPa
203	453	524	14	0.0446	587.3

Here, E, σ_Y, σ_U, A, n, and K are the Young's modulus, yield stress, ultimate strength, elongation at fracture, hardening exponent and hardening coefficient, respectively. The material stress strain behaviour is described by Ludwik's law, /5/, according to:

$$\sigma = K\varepsilon_p^n \tag{1}$$

DEFECT ASSESSMENT

Failure Assessment Diagram (FAD) and SINTAP

In this study, we chose a deterministic approach, derived from SINTAP procedure and FAD. The SINTAP procedure is based on the principle of fracture mechanics and limit analysis; it is used to assess defects in structures, known or assumed. There are several levels of analysis, more and more complex, by allowing the data to obtain a specific result. The lowest level provides the most conservative assessment. All failures in elasto-plastic region are characterised by a point in a FAD, which accounts for any kind of failure: plastic collapse, brittle fracture and elastic-plastic failure, Fig. 2. The FAD presents a failure curve as the critical non-dimensional stress intensity factor versus non-dimensional stress or loading parameter and is applied in several codes referring to structural integrity of cracked structures. The interpolation between two limit states is obtained by a curve representing the fracture limit, called Failure Integrity Line. Many interpolation curves have been proposed. We have chosen to use the curve given by the SINTAP procedure. The mathematical expressions of SINTAP default level procedure is given as, /6/:

$$f(L_r) = \left[1 + \frac{L_r^2}{2}\right]^{\frac{-1}{2}} \left[0.3 + 0.7 \times e^{\left(-0.6 \times L_r^2\right)}\right]$$
$$0 \le L_r \le 1 \; ; \; L_r^{\max} = 1 + \left(\frac{150}{\sigma_Y}\right)^{2.5} \tag{2}$$

where $f(L_r)$, L_r, $L_r^{\max}$ and σ_Y are interpolating function, non-dimensional loading or stress based parameter, the maximal value of non-dimensional loading or stress based parameter and yield stress, respectively. Non-dimensional stress is defined as

$$S_r = \frac{\sigma_g}{\sigma_y} \tag{3}$$

and non-dimensional applied stress intensity factor as

$$K_r = \frac{K_I}{K_{Ic}} \tag{4}$$

where σ_g, σ_y, K_I and K_{Ic} are: gross stress, yield stress, stress intensity factor and critical stress intensity factor.

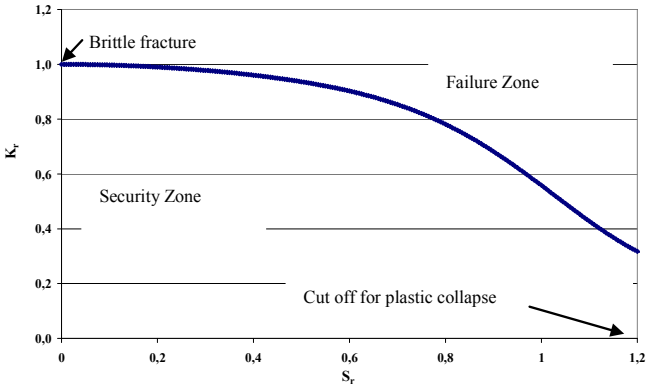

Figure 2. Failure Assessment Diagram.
Slika 2. Dijagram analize otkaza

Point A in Fig. 3 is the assessment point obtained after calculation of two parameters, K_r and S_r. To have the safety factor based on the size of the defect, we need to know two other points, O, origin point of the diagram, and D, point corresponding to the intersection between the Failure Integrity Line and straight line (OA). The value of the safety factor is given by the ratio:

$$f_{s,a} = \frac{OD}{OA} \tag{5}$$

In the same way, we can obtain the security factor, it is to replace the point D by point E, the intersection between the Security Level Line and line (OA).

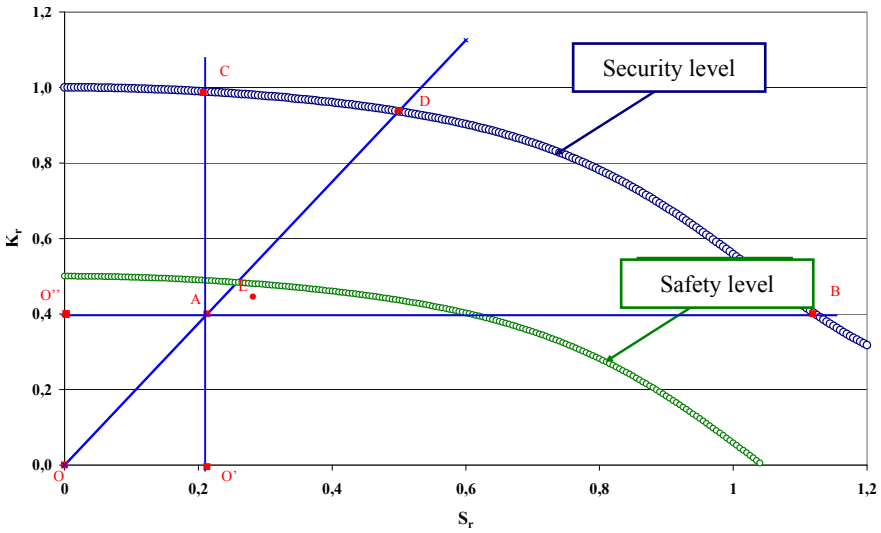

Figure 3. Security factor in a Failure Assessment Diagram.
Slika 3. Faktor bezbednosti u dijagramu analize otkaza

Modified Notch Failure Assessment Diagram (MNFAD)

The SINTAP procedure is only available for one type of defect: cracks. However, the goal of this study concerns the characterisation of defects obtained by external interferences. These defects are considered as notches. Therefore this procedure is adapted, to be used in a Modified Notch Failure Assessment Diagram (MNFAD). The new parameters of the MNFAD are the following:

$$K_{\rho,r} = \frac{K_{\rho,app}}{K_{\rho,c}} \tag{6}$$

$$S_r = \frac{\sigma_{\theta\theta}}{\sigma_0} \tag{7}$$

$$\sigma_0 = \frac{R_e + R_m}{2} \tag{8}$$

where $K_{\rho,app}$, $K_{\rho,c}$, $\sigma_{\theta\theta}$, σ_0, R_e, R_m, are: Notch Stress Intensity Factor (NSIF) applied, critical Notch Stress Intensity Factor, hoop stress, flow stress, yield stress, and ultimate strength, respectively. It is important to emphasize that the toughness obtained through the intensity NSIF is dependent on notch radius. Having a dimensionless parameter, the same failure curve is used whatever the notch radius. The definition of failure integrity line and security factor are the same as for FAD. Operating points in MNFAD are presented by a pair of coordinates (S_r; $K_{\rho,r}$).

Fracture toughness in term of $K_{\rho,c}$

The fracture toughness depends on notch radius. It is well known that the critical stress intensity factor is proportional to the square root of the notch radius below a critical value ρ_{cr}, /7/:

$$K_{\rho,c} = \therefore\sqrt{\rho} \quad \text{for} \quad \rho \geq \rho_{cr} \tag{9}$$

$$K_{\rho,c} = K_{Ic} \quad \text{for} \quad \rho < \rho_{cr} \tag{10}$$

It is to note that fracture toughness measured on specimen with a notch radius greater than ρ_{cr} is denoted $K_{\rho,c}$. This increase of fracture toughness with notch radius is due to the increase of notch plastic zone with notch radius and consequently the increase of total work to fracture. When the notch plastic zone volume is equal to the fracture process zone volume, the notch radius is critical, /8/. It appears necessary to measure the fracture toughness with the corresponding gouge radius. In the following, the notch radius $\rho = 0.15$ mm is accepted as representative of a severe defect and chosen for conservative reasons. This value compared with other obtained from low strength steels is probably below the critical notch radius value. The concept of the critical notch stress intensity factor and corresponding local fracture criterion assume that the fracture process requires a certain fracture process volume, /7/. This local fracture approach is called the Volumetric Method, in which volume is assumed as a cylinder with a diameter called effective distance. Determination of the effective distance is based on bi-logarithmic elastic-plastic stress distribution ahead of the notch because the fracture process zone is the highest stressed zone, characterised by an inflexion point in the stress distribution at the limit of zones II and III in Fig. 4.

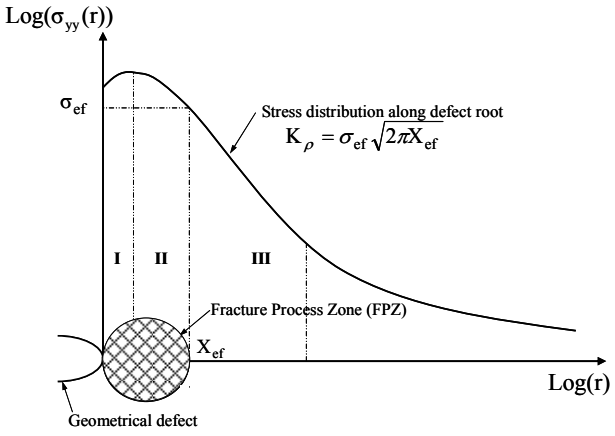

Figure 4. Schematic distribution of elastic-plastic stress ahead of notch tip on notch extension line and the notch stress intensity concept.
Slika 4. Shema raspodele elasto-plastičnog napona ispred vrha zareza na liniji rasta zareza i koncept intenziteta napona zareza

The effective stress σ_{ef} is given as:

$$\sigma_{ef} = \frac{1}{X_{ef}} \int_0^{X_{ef}} \sigma_{yy}(r)\Phi(r)\,dr \qquad (11)$$

and X_{ef}, $\sigma_{yy}(r)$ and $\Phi(r)$ are effective distance, opening stress and weight function, respectively. This stress distribution is corrected by a weight function in order to take into account the distance from notch tip of the acting point and the stress gradient at this point. The effective distance corresponds to the inflexion point with the minimum of the relative stress gradient χ, which can be written as:

$$\chi(r) = \frac{1}{\sigma_{yy}(r)} \frac{\partial \sigma_{yy}(r)}{\partial r} \qquad (12)$$

The effective stress is considered as the average value of the stress distribution within the fracture process zone. The notch stress intensity factor is defined as a function of the effective distance and the effective stress, /7/:

$$K_\rho = \sigma_{ef} \sqrt{2\pi X_{ef}} \qquad (13)$$

and describes the stress distribution in zone III (Fig. 4) as given by the following equation:

$$\sigma_{yy} = \frac{K_\rho}{(2\pi r)^\alpha} \qquad (14)$$

where K_ρ is the notch intensity factor, α is the exponent of the power function of the stress distribution, a constant. Failure occurs when the notch stress intensity factor K_ρ reaches the critical value, i.e. the notch fracture toughness $K_{\rho,c}$, which indicates the resistance to fracture initiation from the notch tip. The stress distribution ahead of the notch tip and along notch ligament can be computed by Finite Element (FE) method for the critical load defined by acoustic emission technique. The critical notch stress intensity factor $K_{\rho,c}$ is calculated using the effective distance and the effective stress obtained from the relative stress gradient, as presented in Fig. 5.

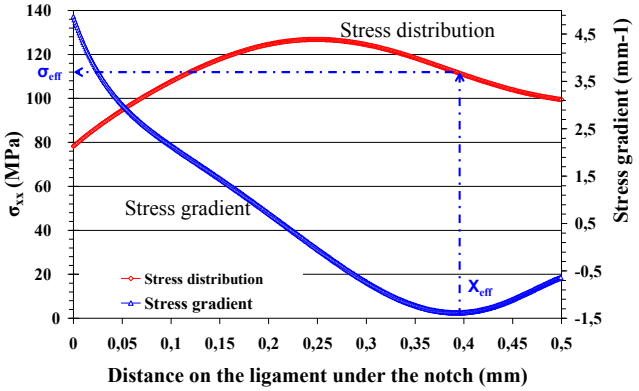

Figure 5. Determination of effective distance using the relative stress gradient method.
Slika 5. Određivanje efektivnog rastojanja primenom relativnog gradijenta napona

TESTS

Burst tests, /9/

Longitudinally notched pipes of diameter D = 219 mm and wall thickness t = 6.1 mm made of X52 steel were tested by bursting under internal pressure (Fig. 6). Environments were 100% dry referenced natural gas (methane) and 100% pure dry hydrogen and free oxygen (less than 1 ppm vol. residual oxygen), in specially designed and manufactured cell with automatic system for pressure and test control as prescribed in Ref. /10/. The test cell (Fig. 7) consists of cylindrical shells: tube-specimen, external cylinder and internal cylinder. Two lids put down the tube-specimen and external cylinder. A special ring seal provides the compression. The external cylinder (d = 375 mm) serves as a protective housing. The axially aligned internal cylinder (d = 165 mm) serves to reduce the hydrogen (or hydrogen/natural gas mixture) bulk volume within testing tube. This is necessary because of safety requirements during the test procedure.

The designed cell enabled an additional space, which is filled with inert gas (argon) for avoiding an emergency situation if leakage of hydrogen/natural gas mixture at the pipe burst occurs. Details of the automatic system for pressure and test control are presented in Fig. 7, with removed protective housing.

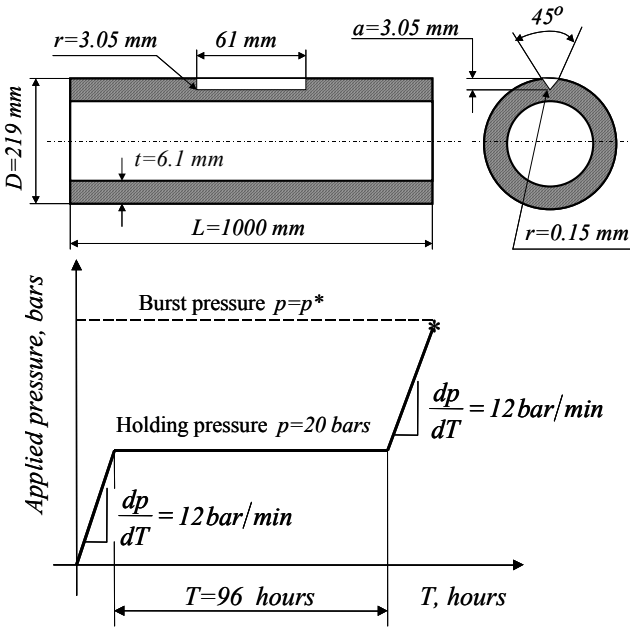

Figure 6. Geometry of notched pipe and burst cycle.
Slika 6. Geometrijski oblik cevi sa zarezom i ciklus raspucavanja

Tests were carried out in specially equipped laboratory, with two separate spaces. First room is used for personnel and operating/controlling equipment. The second room is an intrinsically safe space, where the testing cell is located. Gas-cylinders with hydrogen, natural gas, hydrogen/natural gas mixture and argon are boxed outside of the building. Stainless steel gas pipelines are used (internal diameter d = 6 mm, wall thickness t = 2 mm). Before testing, all pipelines and cavities of the testing cell, cut-off valve and pressure transmitters are purged with argon.

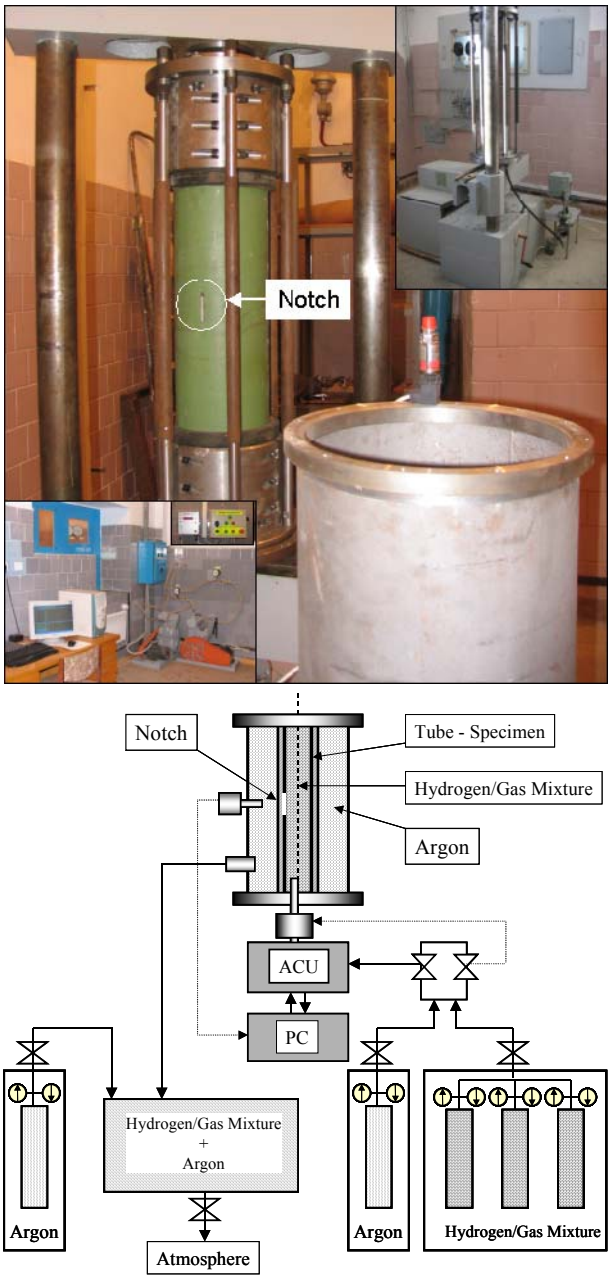

Figure 7. General view of designed testing equipment.
Slika 7. Izgled projektovane ćelije za ispitivanje

This automatic testing system enabled:
- Gas pressure transmission in the cavity of testing pipe under specified rate *dp/dt*.
- Keeping a specified internal pressure in the testing pipe constant during given time *t*.
- Loading of the test pipe by internal pressure under given rate *dp/dt* up to tube burst $p = p^*$.
- Permanent registration of internal pressure $p = \Phi(t)$ in the tube-specimen during test.
- Visualisation of function $p = \Phi(t)$ in real time on the PC monitor for each stage of test.
- Registration and determination of the burst pressure $p = p^*$.
- Permanent registration of pressure on the external tube-specimen surface (space in testing cell filled by argon) during the whole period of the test.
- Venting of the test cell (hydrogen/gas mixture + argon) after the tests are finished.
- Safety valve and outlet of gaseous mixture to atmosphere.

Three point bend tests

For defect assessment of scratches and gouges, it is necessary to determine fracture toughness measured directly on notched specimen, /11/. Non-standard specimen, Roman Tile (RT) type (Fig. 8) was used. The advantage of such a specimen is to allow the fracture test in the radial direction of pipe low thickness and the important curvature.

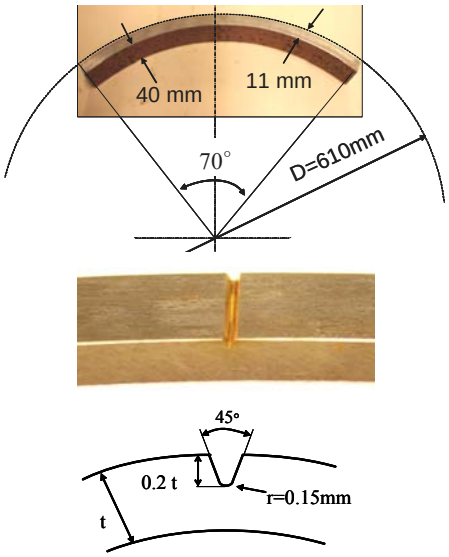

Figure 8. Roman Tile specimen and notch geometry.
Slika 8. Epruveta „rimski crep“ i geometrija zareza

The specimen is loaded in three-point bending through support A and supporting rollers B and C, Fig. 9. Support and rollers are produced of Poly Vinyl Chloride (PVC) to reduce friction. All is monitored at a constant value of 0.02 mm/s. Test duration was of about 30 minutes.

The V-notch with notch opening angle of 45° and root radius of 0.15 mm is machined to a depth the size simulating the expected gouge damage. Test specimens have notch aspect ratio $a/W = 0.2$; W is the wall thickness. A special testing device is developed for this purpose. The bend-test fixture was positioned on the closed loop hydraulic testing machine with a load cell of ±10 kN.

Hydrogen electrolytic charging

The study was conducted in a special soil solution NS4 with pH = 6.7, /12/. Chemical composition of this environment is given in Table 3. In these conditions, i.e. in de-oxygenated, near-neutral pH solution, the hydrogen atoms are generated on the steel surface by electrochemical reduction of water molecules:

$$H_2O + e \rightarrow H_{ads} + OH^- \quad (15)$$

Adsorbed hydrogen atoms can subsequently combine into H_2 molecules by the chemical reaction:

$$2\,H_{ads} \rightarrow H_2 \quad (16)$$

or the electrochemical reaction:

$$H_{ads} + H_2O + e \rightarrow H_2 + OH^- \quad (17)$$

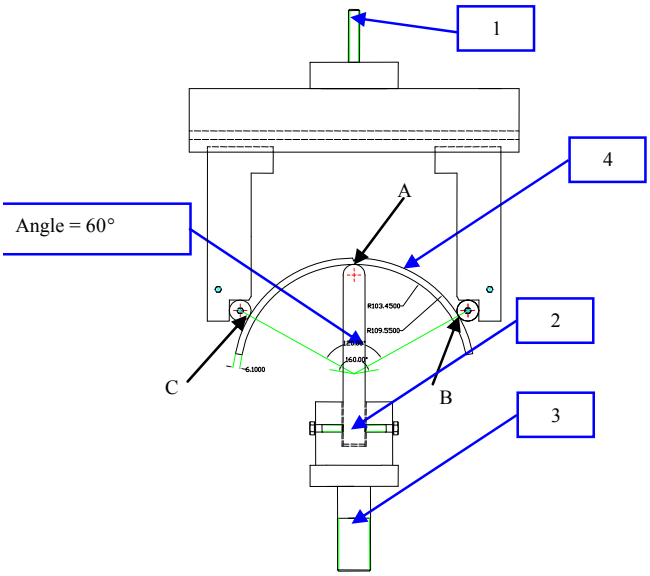

Figure 9. Roman Tile specimen fixture and assembly: 1–connection with load cell; 2–transmitting component with rounded tip; 3–connection of test assembly with the testing machine bottom; 4–"Roman tile" specimen.
Slika 9. Nosač i sklop za ispitivanje epruvete "rimski crep": 1–veza sa opteretnom ćelijom; 2–komponenta za prenos opterećenja sa zaobljenim vrhom; 3–veza ispitnog sklopa sa donjim delom mašine; 4–epruveta "rimski crep"

Table 3. Chemical composition of NS4 solution, gram/litre, /12/.
Tabela 3. Hemijski sastav rastvora NS4, gram/litar, /12/

$NaHCO_3$	KCl	$CaCl_2$	$MgCl_2 \cdot H_2O$
0.483	0.120	0.137	0.131

Here should be noted that the absorbed hydrogen atom concentration under the cathodic polarisation depends on the hydrogen atom recombination mechanisms. When the chemical reaction Eq. (16) dominates in the hydrogen atom recombination, the applied cathodic polarisation enhances the generation of hydrogen atoms and thus the amount of hydrogen atoms penetrating into the steel. The absorbed hydrogen atom concentration will increase continuously with cathodic polarisation potential. In the case of electrochemical reaction, Eq. (17), dominating the hydrogen atom recombination, the cathodic polarisation promotes the generation of hydrogen atoms through reaction Eq. (15), and simultaneously, enhances the hydrogen atom recombination through reaction Eq. (17). Thus, the role of cathodic polarisation is to generate hydrogen atoms and also to recombine hydrogen atoms. Accounting the fact that a steady state condition of hydrogen charging cannot be imposed nor obtained in a freely corroding situation, here the following procedure is made. Specimens are hydrogen charged at constant polarisation potential $E_{cath} = -1000$ mV_{SCE}, which is slightly more negative for tested steel than free corrosion potential $E_{corr} = -800$ mV_{SCE}. Specimens were immersed into the cell with special NS_4 solution and exposed under constant potential of polarisation, E_{cath}. The surface of auxiliary electrode was parallel to notch plane with the distance $h = 20$ mm.

RESULTS

Fracture toughness

Critical load is detected by acoustic emission as for tests in air, and hydrogen condition, /11/. The acoustic sensors have been protected against corrosion for tests under hydrogen electrolytic. This critical load is then introduced in a FE code to compute notch tip stress distribution. Then effective stress and effective distance are combined through the Volumetric Method to obtain the critical notch stress intensity factor. Finite Element computing is made with the same stress strain curve as for air because:

– there is only a slight difference of the behaviour in air and in the presence of hydrogen for small strain,
– the hydrogen affected volume is small compared with the total volume of specimens.

Eleven tests have been performed in air condition, and four in hydrogen electrolytic condition (with 2 different exposition times, 145 and 330 hours). Obtained results are given in Table 4.

Table 4. Notch fracture toughness in term of $K_{\rho c}$.
Tabela 4. Žilavost loma zareza iskazana kao $K_{\rho c}$

	Air	145 hours	330 hours
$K_{\rho c}$ (MPa√m)	57.21	47.68	41.78

Burst pressure

Test results showed that burst pressure for test in methane is $p_{max} = 118$ bar and in hydrogen $p_{max} = 118$ bar. Therefore, there is no gaseous hydrogen effect on the strength of notched pipes for considered testing conditions.

Mechanical properties under hydrogen electrolyte

Tensile specimens are used to characterise mechanical properties of this steel in two environments, air and electrolytic hydrogen. Only a small part of the specimen was opened to be charged with hydrogen, Fig. 10.

The ultimate strength is negligibly affected by hydrogen concentration. However, the elongation at fracture is considerably reduced, as can be seen in Table 5.

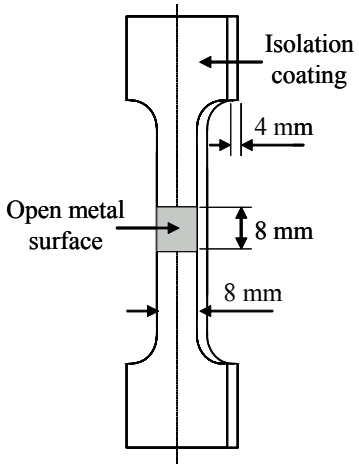

Figure 10. Specimen used in hydrogen charging.
Slika 10. Epruveta za izlaganje dejstvu vodonika

Table 5. Influence of hydrogen concentration on tensile properties of X52 steel.
Tabela 5. Uticaj koncentracije vodonika na zatezne karakteristike čelika X52

Environment	Yield stress	Ultimate strength	Elongation at fracture
	R_e (MPa)	R_m (MPa)	A_f (%)
Air	453	524	14.03
Hydrogen	479	547	11.44

Security and safety factors

Using the values, given in Tables 6 and 7, the MNFAD are calculated, applying derived formulae.

Graphical presentation of Modified Notch Failure Assessment Diagram as presented in Fig. 11.

The safety factor for the same defect and for the same service conditions, one for material without hydrogen embrittlement, the second with hydrogen embrittlement are then established (Fig. 11). Hydrogen embrittlement leads to a reduction of the safety factor for 18.33%.

Table 6. Obtained values of effective distance, effective stress, notch stress intensity factor and hoop stress for given conditions.
Tabela 6. Vrednosti efektivnog rastojanja, efektivnog napona, faktora intenziteta napona zareza i obimskog napona za date uslove

Effective distance	Effective stress	Notch stress intensity factor	Hoop stress
X_{ef} (mm)	σ_{ef} (MPa)	K_ρ (MPa√m)	$\sigma_{\theta\theta}$ (MPa)
0.67	343	15.8	125

Table 7. Average values of material properties with and without hydrogen effect; calculated values of parameters k_r and S_r.
Tabela 7. Prosečne vrednosti karakteristika materijala pod uticajem i bez uticaja vodonika, sračunate veličine parametara k_r i S_r

Environment	Notch fracture toughness	Flow stress	Notch stress intensity factor ratio	Stress ratio
	$K_{\rho,c}$	$\sigma_0 = (\sigma_u+\sigma_T)/2$	$k_\rho = K_\rho/K_{\rho,\chi}$	$S_r = \sigma_{\theta\theta}/\sigma_0$
	MPa√m	MPa	–	–
Air	57.21	496	0.276	0.252
Hydrogen	44.73	513	0.35	0.244

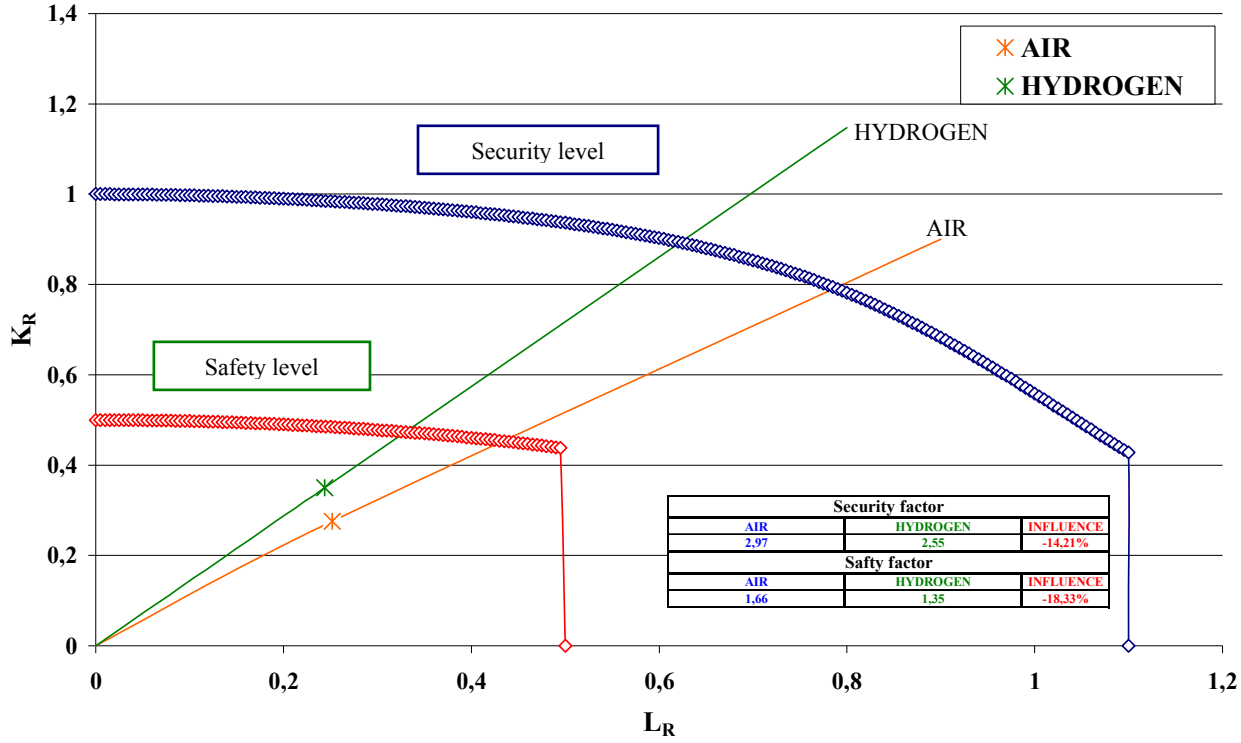

Figure 11. Modified Notch Failure Assessment Diagram (MNFAD).
Slika 11. Modifikovani dijagram za ocenu analize otkaza zbog zareza

In the hydrogen environment, the security factor decreases by 14%, but its value is always over the conventional value of 2. The safety factor is somewhat more affected, 18%. In severe conditions, hydrogen electrolytic, the decreasing of the different factor, is acceptable.

CONCLUSIONS

To assess the harmfulness of a pipe surface defect such as a gouge, a Modified Notch Failure Assessment Diagram (MNFAD) is established based on the Volumetric Method (VM) of notch fracture mechanics. This MNFAD is coupled with the SINTAP failure curve and allows determining the safety factor associated with defect geometry, loading conditions and material resistance. Determination of the assessment points requires determining the fracture toughness in radial pipe direction of low thickness and high curvature. This is done using a special specimen, the Roman Tile. Tensile properties are measured by electrolytic hydrogen charging method.

The obtained data coupled with the MNFAD method lead to the conclusion that in presence of a severe surface gouge defect, the reduction of the safety factor is 14%, but remains over the conventional value of 2. These results indicate the possibility to use the existing European natural gas pipe network for the transport of a mixture of natural gas and hydrogen.

REFERENCES

1. Fernandes, T.R.C., da Graça Carvalho, F.C., *"Hy Society" in support of European hydrogen projects and EC policy*. International Journal of Hydrogen Energy, 30 (2005), pp.239-245.
2. Mulder, G., Hetland, J., Lenaers, G., *Towards a sustainable hydrogen economy: Hydrogen pathways and infrastructure*, Inter. J of Hydrogen Energy, 32, Issues 10-11 (2007), pp.1324-1331.
3. NaturalHy Project, http://www.naturalhy.net
4. Rapport de l'enquête MH-2-95, "Fissuration par corrosion sous tension des oléoducs et des gazoducs canadiens", Office National d'Energie, (1996).
5. Capelle, J., Dmytrakh, I., Gilgert, J., Jodin, Ph., Pluvinage G., *A comparison of experimental results and computations for cracked tubes subjected to internal pressure*, Materials and Technology 40, pp.233-237, (2006).
6. SINTAP: Structural Integrity Assessment Procedure, Final Report E-U project BE95-1462 Brite Euram Programme Brussels (1999).
7. Pluvinage G., Fracture and Fatigue Emanating from Stress Concentrators; Kluwer, (2003).
8. Akourri, O., Louah, M., Kifani, A., Gilgert, G., Pluvinage, G., *The effect of notch radius on fracture toughness J_{Ic}*, Eng Fract Mech 65, pp.491-505, (2000).
9. Capelle, J., Gilgert, J., Dmytrakh, I., Pluvinage, G., *Sensitivity of pipelines with steel API X52 to hydrogen embrittlement*, Inter. J of Hydrogen Energy 33, issue 24, pp.7630-7641, (2008)
10. Burst tests on pipes under pressure of mixture of hydrogen and natural gas. Final report on Subcontract No 1401-2005 of NATURALHY-Project (Contract No SES6/2004/502661). Karpenko Physico-Mechanical Institute of National Academy of Sciences of Ukraine, Lviv, Ukraine (2006).
11. Capelle, J., Gilgert, J., Dmytrakh, I., Pluvinage, G., *Hydrogen effect on fatigue and fracture resistance of a pipe steel*, Structural Integrity and Life, Vol.9, No1, 2009, pp.9-14.
12. Capelle, J., Dmytrakh, I., Pluvinage, G., *Electrochemical Hydrogen Absorption of API X52 Steel and its Effect on Local Fracture Emanating from Notches*, Structural Integrity and Life, Vol.9, No1, 2009, pp.3-8.